Supplementary Materials and Methods

Antibody information

Primary antibodies used were mouse monoclonal anti-acetylated α-tubulin (Sigma; 1:800), mouse monoclonal or rabbit polyclonal anti-γ-tubulin (Sigma; both at 1:100), rabbit anti-Vangl2 (Montcouquiol et al., 2006, 1:500), mouse anti-β2-spectrin (BD Transduction Laboratories, 1:300), anti-BBS2 (Protein Tech Europe, 1 in 50-100), anti-Ift20 (G.Pazour, 1 in 300), rabbit polyclonal anti-Gαi3 (Sigma G4040, 1 in 600). Secondary antibodies were Alexa Fluor 488 or 568 tagged secondary antibodies (Molecular Probes; 1:1000). Actin was labeled with phalloidin-546 (Sigma; 1:200).

Quantification of cochlea and utricle polarity defects

The position of the kinocilium (proximal end) was mapped by labeling with acetylated tubulin or basal body labeled with gamma tubulin. Bundle positioning was annotated by marking the center of the bundle. P0 utricles were dissected and immunostained for β2-spectrin. A cluster of 25 utricle hair cells were chosen in comparable regions of the lateral extra-striolar domain of mutant and control mice. The orientation of each hair cell was measured relative to neighboring cells based upon β2-spectrin labeling. The angle difference between each hair cell and its neighboring cells was calculated and average angle difference and standard deviation of angle difference were averaged.

Immunogold labeling and transmission electron microscopy (TEM)

For postembedding immunogold, cochleae were fixed in 4% paraformaldehyde + 0.5% glutaraldehyde in 0.1 M phosphate buffer, and further processed using established methods (Petralia et al., 2010; Petralia and Wenthold, 1999). Following cryoprotection, tissue was frozen in liquid propane in a Leica CPC freezing instrument, and tissue was processed and embedded at low temperature in Lowicryl HM-20 resins, using a Leica AFS freeze-substitution instrument. Thin sections from this material were incubated in primary antibody after blocking, and then in 10 nm-gold conjugated secondary antibody. Finally, sections were stained with uranyl acetate and lead citrate and examined in a JEOL 1010 transmission electron microscope. Control sections lacking the primary antibody, from 2 animals, showed only rare gold labeling. For the ventricular zone/choroid plexus immunogold studies in the supplement, images were taken in areas of these structures just dorsal (ventricular zone of lateral ventricle) and rostral (choroid plexus) to the hippocampus in parasagittal sections of

the brain of P37 and P2 rats, respectively; this tissue has been used and characterized for postembedding immunogold previously (Petralia et al., 2011; Petralia et al., 2010).

Affymetrix microarray analyis

Target labeling and hybridization to GeneChips were carried out in the NIDDK Microarray Core facility using the GeneChip Mouse 430_2 Array purchased from Affymetrix. Samples from each genotype were pooled and split onto two chips each. The microarray signals were normalized using the RMA algorithm. The significantly differentially expressed genes were selected based on an ANOVA using the Partek Genomics Suite software (Partek, St. Charles, MO, USA). The ANOVA gene lists with P value less than 0.05 and absolute value of fold change greater than 2, were used for biological interpretation using Partex Pathway analysis.

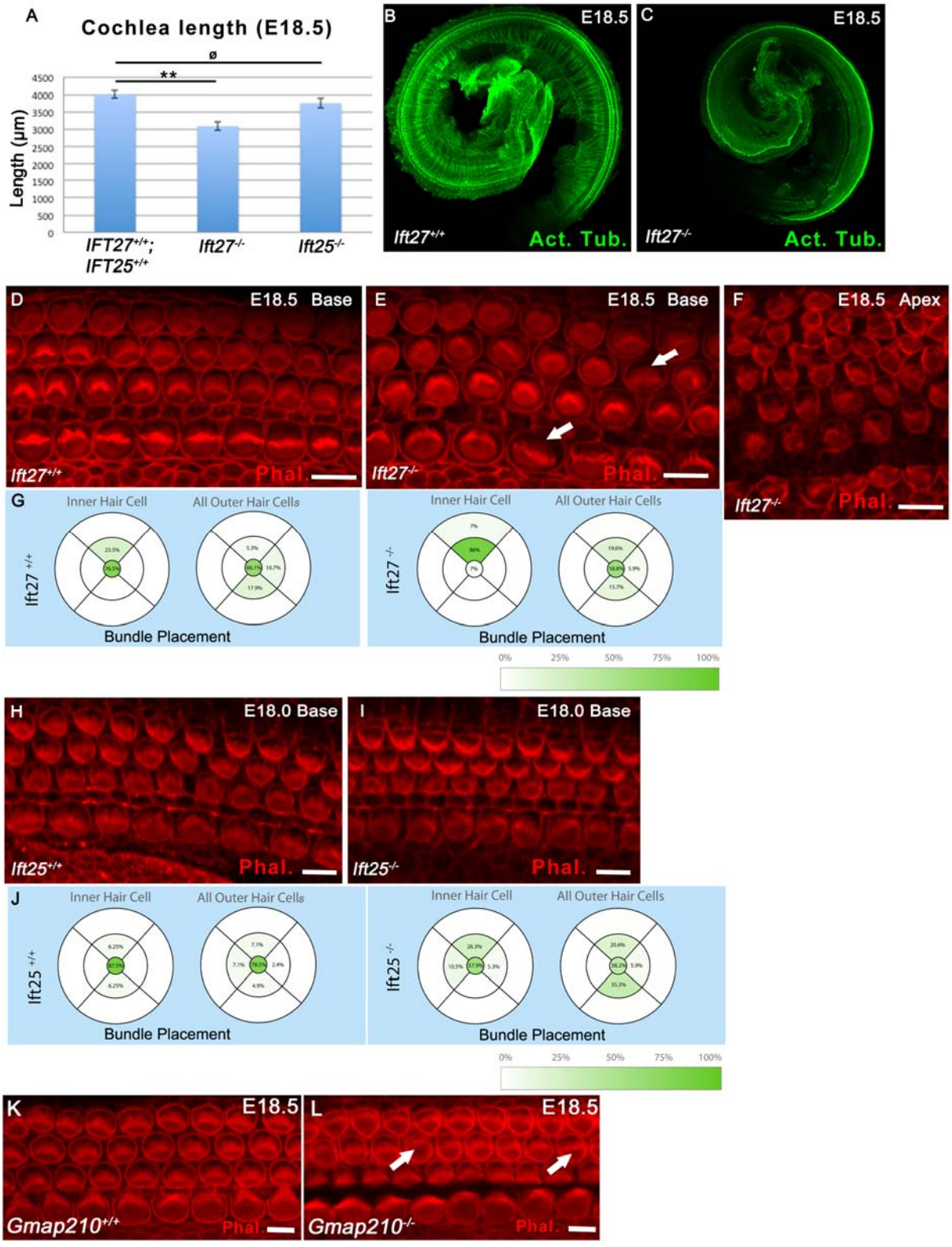

Supplementary Figure 1. Analyses of cochleae from *Ift25*$^{-/-}$, *Ift27*$^{-/-}$, and *Gmap210*$^{-/-}$ mutants. **A-C.** At E18.5 cochlear length is significantly shortened in *Ift27*$^{-/-}$ cochleae compared to controls. *Ift25*$^{-/-}$ cochleae are not significantly different from controls (n>5). Statistical analysis was done using a two-tailed Student's t-test. Statistical significance of the

data is represented as: (ø) non-significant; (**) $p<0.01$. Error bars are S.D. **B, C** Whole mount images of cochleae from WT and *Ift27*$^{-/-}$ mice at E18.5 labeled with an antibody against acetylated tubulin. The length of the *Ift27*$^{-/-}$ cochlea is approximately 75% of WT. **D-L.** Surface views of cochlear whole mounts from *Ift27*$^{-/-}$, *Ift25*$^{-/-}$ and littermate controls at E18.5 and summaries of bundle orientations. **D-F.** Only mild stereociliary bundle defects (phalloidin; red) are present in *Ift27*$^{-/-}$ cochleae. However, as would be expected in a shortened cochlea, increased rows of hair cells are present in the apex. **G.** Graphical summary of bundle positioning in *Ift27*$^{-/-}$ cochleae. Overall bundle positions are comparable to control. **H-L.** Bundle positions and shapes in cochleae from *Ift25*$^{-/-}$ and *Gmap210*$^{-/-}$ mice appear unchanged by comparison with WT, with only few hair cells exhibiting flattened bundles (white arrows). Scale bars are 5 μm

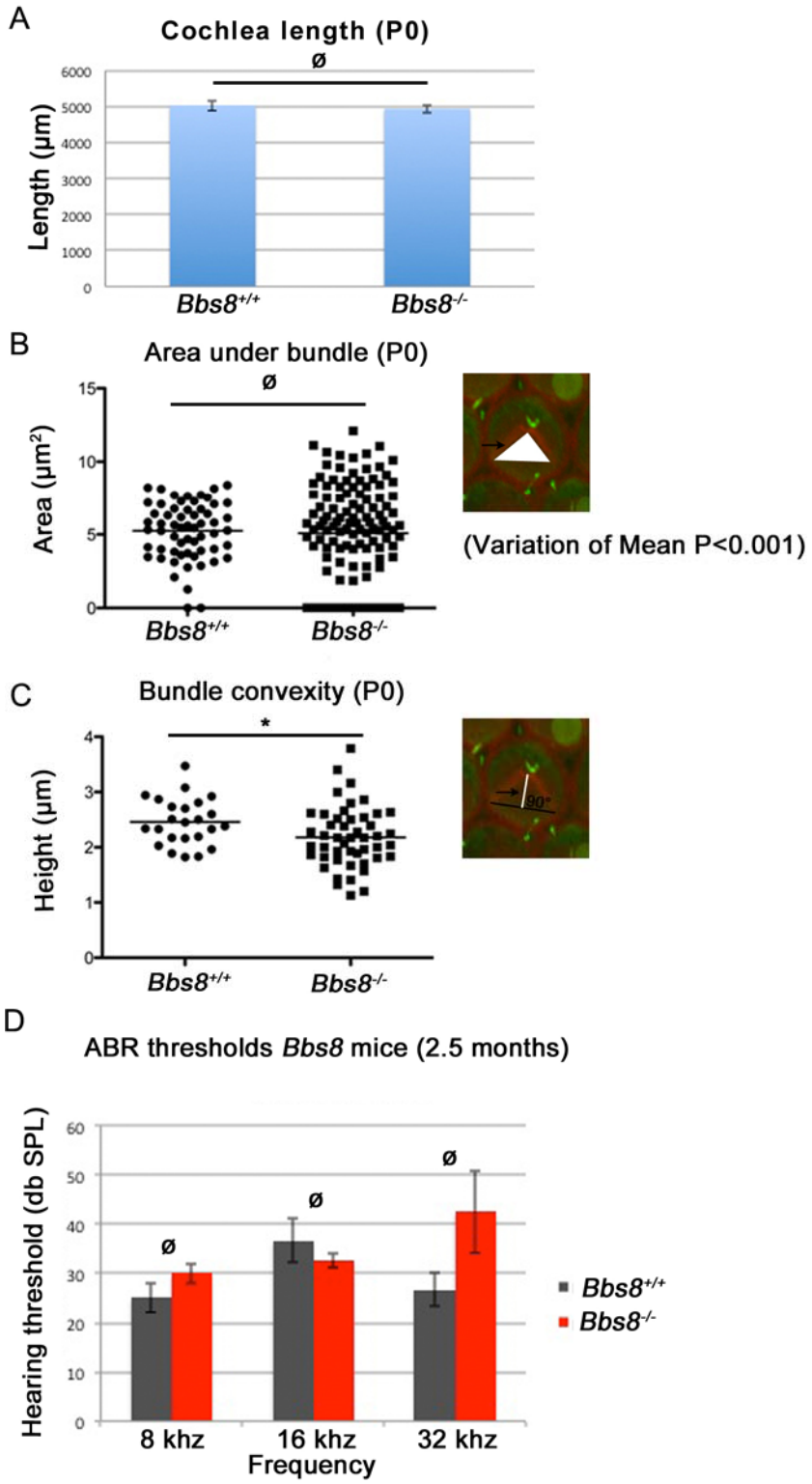

Supplementary Figure 2. Additional analyses of defects in *Bbs8*$^{-/-}$ cochleae. **A.** Cochlea length in *Bbs8*$^{-/-}$ mutants at P0 compared to control (n=6). No differences are observed. **B**. Quantification of the area encompassed by the arms of outer hair cell stereociliary bundle (see inset) in *Bbs8*$^{+/+}$ and *Bbs8*$^{-/-}$ in the basal turn of P0 cochleae, graphed as a scatter plot.

While the overall area mean is not significantly different (p=0.72), there is a much greater degree of variation for bundles from *Bbs8*$^{-/-}$ cochlea (p<0.001). C) Measurement of bundle convexity (height) in P0 *Bbs8*$^{+/+}$ and *Bbs8*$^{-/-}$ mammalian cochleae (basal turn), graphed as a scatter plot. Mean convexity is significantly lower in *Bbs8*$^{-/-}$ cochleae (p=0.032). C) Initial ABR recordings (up to 32 Khz, tested on Intelligent Hearing Systems) in 2-3 month *Bbs8+/+* and *Bbs8-/-* mice. We see no significant difference in ABR thresholds at lower frequencies. Two-way comparisons were done using a non-parametric, unpaired t-test (Mann Whitney). Statistical significance of the data is represented as: (ø) non-significant; (*) p<0.05. Error bars are S.D.

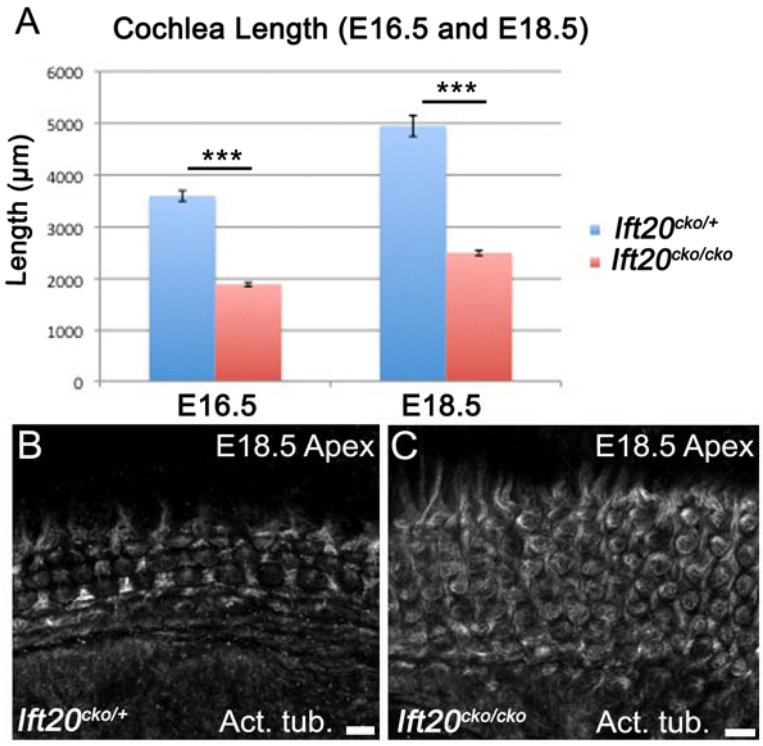

Supplementary Figure 3. Cochlea extension defects in *Ift20*$^{cko/cko}$ cochleae. A) Bar chart showing cochlear length at E16.5 and E18.5 is significantly shortened in *Ift20*$^{cko/cko}$ cochleae compared to controls (n>6). Two-way comparisons were done using a non-parametric, unpaired t-test (Mann Whitney). Statistical significance of the data is represented as: (***) p<0.001. Error bars are S.D. B, C) Immunohistochemistry of *Ift20*$^{cko/+}$ and *Ift20*$^{cko/cko}$ cochlear apex at E18.5 using an antibody against acetylated α-tubulin (green). Expansion of the sensory epithelium with extra rows of hair cells (as seen by acetylated α-tubulin labeling) is seen in *Ift20*$^{cko/cko}$ cochleae. Scale bars are 5 µm.

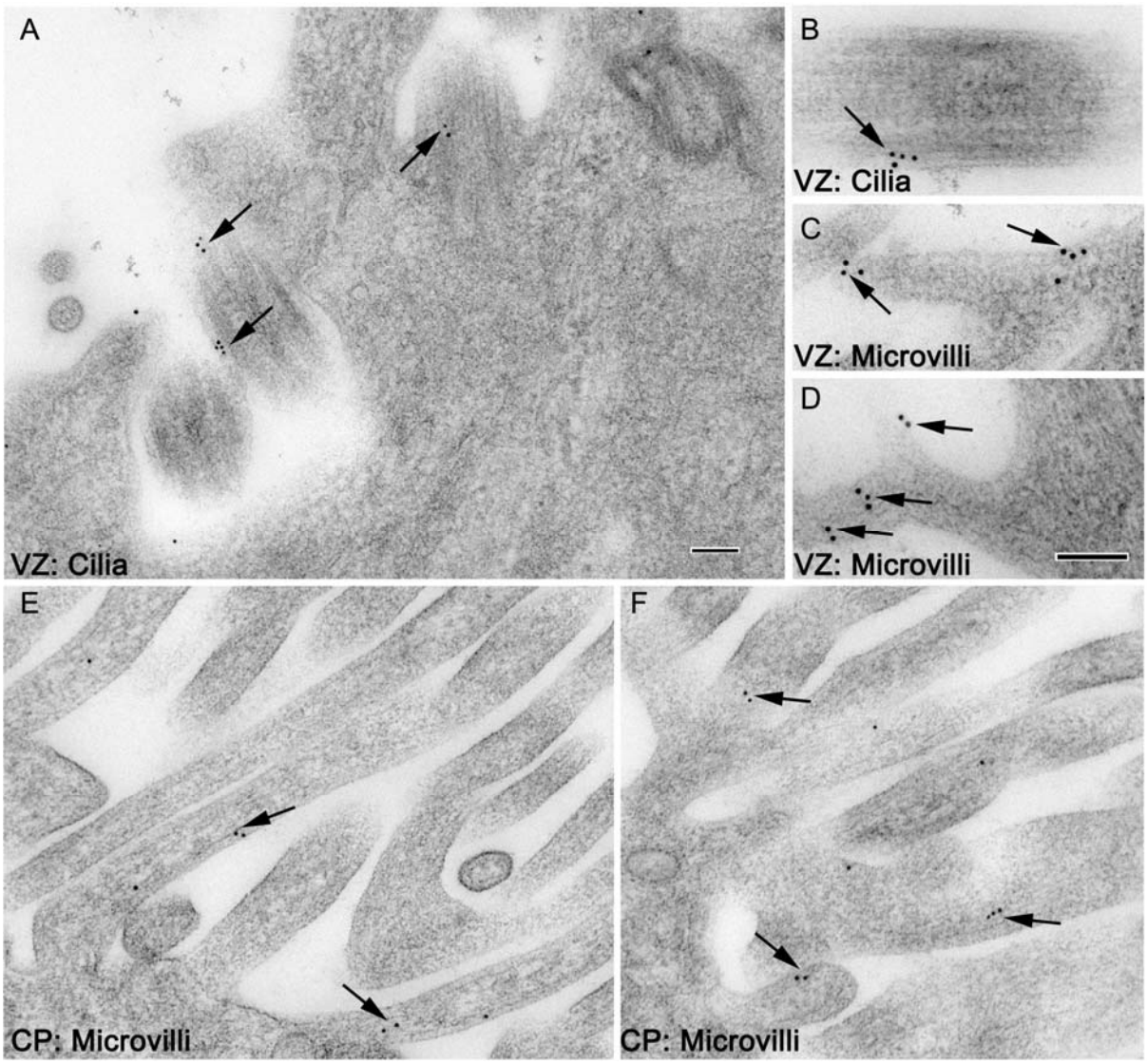

Supplementary Figure 4. Immungold labeling for Bbs2 in the ventricular zone of the P37 rat (A-D) and the choroid plexus of the P2 rat (E, F). Note the clusters of gold in cilia in A and B, microvilli in C and D, and the specialized microvilli of the choroid plexus (E and F). VZ: Ventricular zone; CP: Choroid Plexus Scale bar is 100 nm (in A for A, E, and F; in D for B-D).

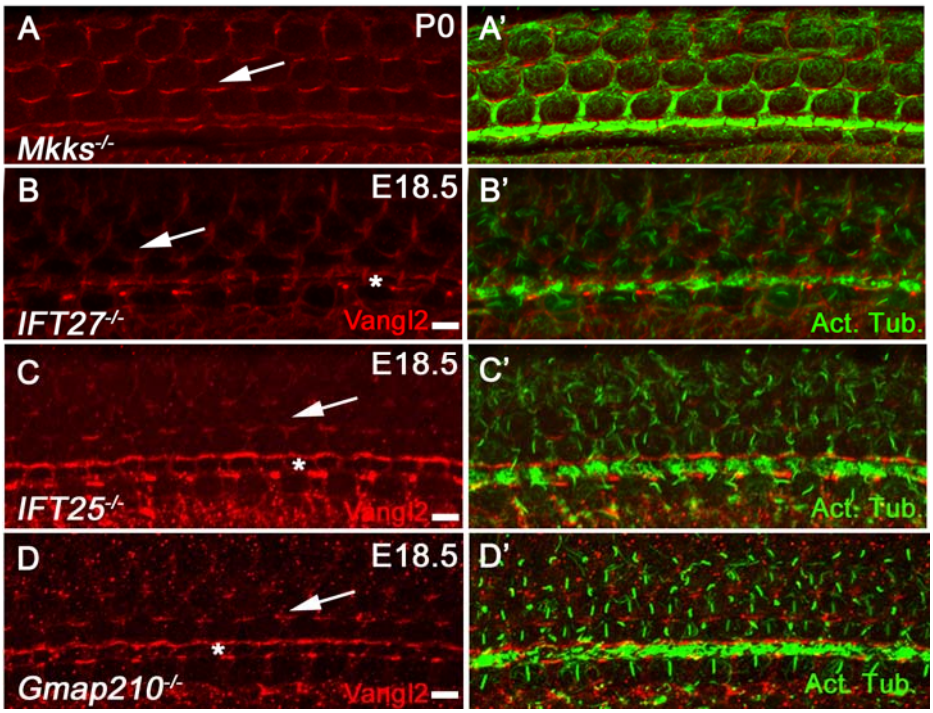

Supplementary Figure 5. Regular Vangl2 localization in other cilia mutants. A-D) Localization of Vangl2 (red) and acetylated α-tubulin (green) in basal turn of Bbs6/Mkks$^{-/-}$,*Ift27*$^{-/-}$, *Ift25*$^{-/-}$ and *Gmap210*$^{-/-}$ at P0. Staining along the pillar cells and hair cell boundaries is comparable to controls. (See Figure 7A and C for control) Scale bars are 5 μm.

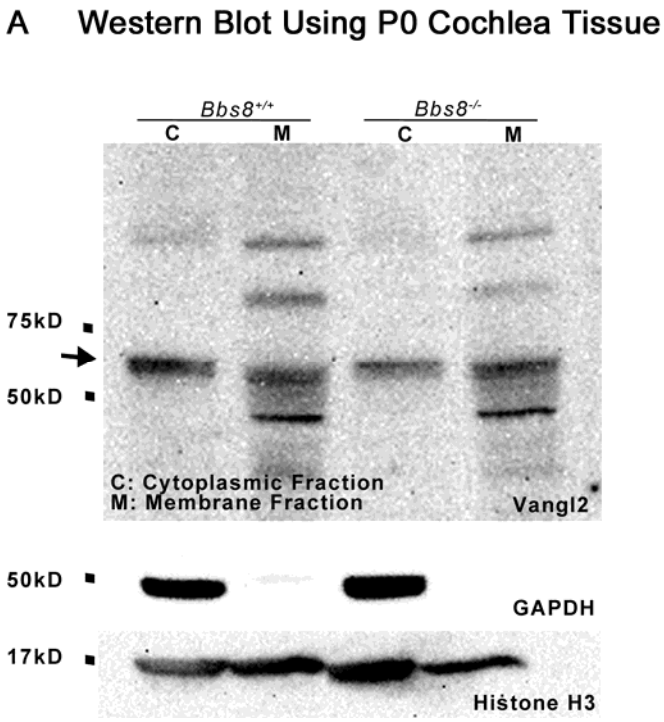

Supplementary Figure 6. Vangl2 expression via western blot. A. Serial cytoplasmic (PBS extracted) and membrane (Ripa buffer extracted) factions from *Bbs8*$^{+/+}$ and *Bbs8*$^{-/-}$ cochleae. Western blot probed with antibody against Vangl2. No significant difference observed between control and mutants in either fraction (Supplementary Figure 6). Six cochleae (P0) were pooled for protein extraction. GAPDH and Histone H3 were used as loading control.

Table S1.

Click here to Download Table S1